Appl Nanosci (2016) 6:951–957
DOI 10.1007/s13204-015-0511-x

ORIGINAL ARTICLE

Biological applications of zinc imidazole framework through protein encapsulation

Pawan Kumar[1] · Vasudha Bansal[1] · A. K. Paul[2] · Lalit M. Bharadwaj[3] · Akash Deep[2] · Ki-Hyun Kim[1]

Received: 27 July 2014 / Accepted: 16 November 2015 / Published online: 1 December 2015

Abstract The robustness of biomolecules is always a significant challenge in the application of biostorage in biotechnology or pharmaceutical research. To learn more about biostorage in porous materials, we investigated the feasibility of using zeolite imidazolate framework (ZIF-8) with respect to protein encapsulation. Here, bovine serum albumin (BSA) was selected as a model protein for encapsulation with the synthesis of ZIF-8 using water as a media. ZIF-8 exhibited excellent protein adsorption capacity through successive adsorption of free BSA with the formation of hollow crystals. The loading of protein in ZIF-8 crystals is affected by the molecular weight due to diffusion-limited permeation inside the crystals and also by the affinity of the protein to the pendent group on the ZIF-8 surface. The polar nature of BSA not only supported adsorption on the solid surface, but also enhanced the affinity of crystal spheres through weak coordination interactions with the ZIF-8 framework. The novel approach tested in this study was therefore successful in achieving protein encapsulation with porous, biocompatible, and decomposable microcrystalline ZIF-8. The presence of both BSA and FITC–BSA in ZIF-8 was confirmed consistently by spectroscopy as well as optical and electron microscopy.

Keywords Zeolitic imidazolate framework (ZIF-8) · Proteins · BSA · Successive adsorption

Introduction

Proteins are natural and fundamental bio-functional units consisting of one or more chains of amino acids. They play many biological roles, such as catalysts with enhanced reactivity, selectivity, and specificity under mild conditions. If immobilized on a solid and porous surface, proteins can exhibit prolonged biological functioning (Pinto Reis et al. 2006; Gao et al. 2009; Lee et al. 2010; Worsdoorfer et al. 2012). In this regard, a great deal of attention has been drawn to the porous materials used as support due to their potential for interaction with proteins (Pinto Reis et al. 2006; Gao et al. 2009; Lee et al. 2010; Worsdoorfer et al. 2012). Nonetheless, development of these materials faces major challenges by insufficient stability of encapsulated proteins, e.g., incomplete release or initial burst release. It is widely perceived that chemical and mechanical stress are produced during the process of microencapsulation and that a longer duration of storage can increase damaging effects on the conformational and biological integrity of the protein (Yeo and Park 2004). Moreover, application of protein encapsulation for sensing also has challenges and difficulties due to reductions in (a) sensitivity, (b) activity, (c) operational stability, (d) recovery, and (e) reusability under certain experimental conditions (Such et al. 2011; Danhier et al. 2012). Consequently, there is a need for more research on the build-up of multi functionality platforms for proteins to overcome these major limitations.

Electronic supplementary material The online version of this article (doi:10.1007/s13204-015-0511-x) contains supplementary material, which is available to authorized users.

✉ Pawan Kumar
pawannano10@gmail.com

[1] Department of Civil and Environmental Engineering, Hanyang University, 222 Wangsimni-Ro, Seoul 133-791, Republic of Korea

[2] Central Scientific Instruments Organisation (CSIR-CSIO), Sector 30 C, Chandigarh 160030, India

[3] Amity Institute of Nanotechnology, Noida, India

The incorporation of biomolecules or nanomaterials on metal organic frameworks (MOFs) has attracted a great deal of interest because of their potential for clinical, health, and environmental applications due to the novel chemical, physical, and optical properties of those materials (Czaja et al. 2009; Chen et al. 2010; Lohe et al. 2011; Danhier et al. 2012; Liu 2012). MOFs are the structural analogs of zeolites, but are different in terms of their stability, selectivity, porosity, and especially feasibility of building a crystal structure. Development of MOFs has thus been remarkably achieved in various fields of study including catalysis, nonlinear optics, separation, magnetism, fluorescence, gas storage, ion exchange, and others (Allendorf et al. 2009; Buso et al. 2011; Sugikawa et al. 2011; Tsuruoka et al. 2011).

Recently, the synthesis and design of zeolitic imidazolate framework (ZIF-8) have been favored following the recognition of its interatomic potential, topologies, framework architectures, large cavities (11.6 Å at window size of 3.4 Å), and chemical/thermal stability (Watson et al. 2002; Park et al. 2006; Phan et al. 2010; McKinlay et al. 2010; Springuel-Huet et al. 2013). This large window size of ZIF-8 allows greater flexibility to accommodate large guest molecules in the support material. In this respect, much of the current knowledge is based on the pioneering work of Lu et al. (2012), who demonstrated the encapsulation of nanoparticles in ZIF-8 (as molecular sieving) with the same functional characteristics as those of the isolated nanoparticles (Lu et al. 2012).

Here, we present the first report of a protein encapsulation strategy in ZIF-8, to the best of our knowledge. To this end, the incorporation (or immobilization) of biomolecules (or protein) was achieved within Zeolitic imidazolate framework material (ZIF-8). This fundamental strategy was used for the development of the synthesis of ZIF-8 in an aqueous medium in the presence of BSA, a model protein.

Experimental

Materials

All of the solvents and reagents, including zinc nitrate hexahydrate (Merck), methyl imidazolate (Merck), trimethyl ethyl amine (TEA), bovine serum albumin, and FITC–BSA (Sigma-Aldrich), were purchased as analytical grade and used as received. The UV–Vis spectroscopy (Varian Cary 500) was carried out in the range of 200–3300 nm. The synthesis and confirmation of crystal formation was done using X-ray diffraction (Shimadzu, 6000 diffractometer). Topological studies were performed using a confocal microscope, scanning electron microscope (SEM), and transmission electron microscope (TEM). The conjugate formation was confirmed by FTIR spectroscopy (Thermo-2400).

ZIF-8 synthesis and encapsulation of BSA

To prepare ZIF-8 in aqueous medium, we followed the synthesis procedure of Watson et al. (2002), as shown in Fig. 1a, b (Watson et al. 2002; Kida et al. 2013). The same procedure described by this group was used to encapsulate the BSA and FITC–BSA in ZIF-8. This FITC–BSA experimental study was carried out to confirm the encapsulation of BSA in ZIF-8 by confocal microscopy. The detailed procedures of synthesis and encapsulation are

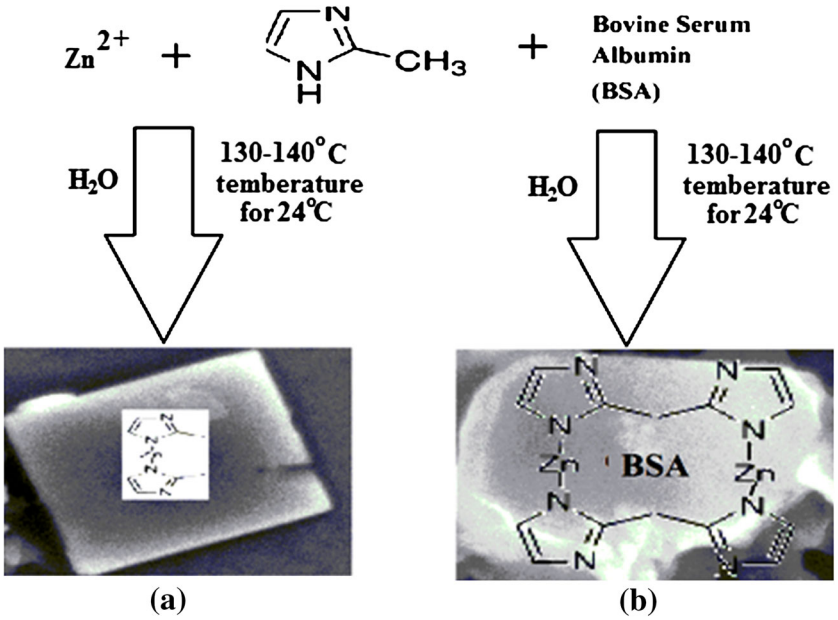

Fig. 1 Protein (BSA) incorporation in ZIF-8 scheme: SEM image, **a** ZIF-8 blank crystal and **b** ZIF–BSA composite. Bovine serum albumin (BSA) of size 2–4 nm with globular shape was well dispersed in ZIF-8 crystals due to assembly of zinc ions with imidazolate ligand

described in the supporting information (Table 1 and Section S2.2.1–S2.2.2).

Results

ZIF-8 was synthesized in the presence of BSA in aqueous solution at the ratio 3:1 (Fig. 1). Milky crystals were obtained by combining the BSA and ZIF-8. The product was centrifuged and washed several times with distilled water. Transmission and scanning electron microscopy images and IR spectroscopy analyses showed the resultant cubic polyhedral crystal of ZIF-8 together with multiple BSA molecules. However, no free BSA was observed during the analyses. The supernatant was transparent and colorless, and the UV–Vis absorption spectrum showed no detectable peaks. These observations indicate that after the final reaction, all of the BSA was incorporated into the crystal structures of ZIF-8. The analysis of confocal microscopic images of the composite material obtained just after 24 h revealed the reaction of BSA–FITC with ZIF-8. The crystals were composed of organic and inorganic molecules as well as embedded and adsorbed BSA molecules, according to the confocal laser scanning microscope (CLSM) and electron microscopy analyses.

X-ray diffraction analysis

X-ray diffraction pattern analysis was performed on an XRD diffractometer (Shimadzu, 6000) with graphite monochromatic Cu-Kα radiation ($\lambda = 1.54$ Å) at room temperature. The crystal structure of ZIF-8 was analyzed by direct method and by optimized structure, as reported in the literature. The calculations were performed at B3LYP/6-31 + G (d) level of DFT theory of Gaussian 3.0 with atomic coordinates and thermal anisotropic parameters for all non-hydrogen atoms (Watson et al. 2002; Pan et al. 2011; Gross et al. 2012; Kida et al. 2013). Carbons and hydrogens of crystalline structures were included in the calculation of structure factor at idealized positions using the basic set B3LYP/6-31 + G (d) level of DFT theory. The crystal structure X-ray diffraction patterns of ZIF-8 and ZIF–BSA are shown in Fig. 2. The different parameters including the 2θ, D-spacing, and Miller indices were as follows (A) ZIF-8: cubic, $a = 16.4110$ (1) Å; $V = 4378.73$ (6) Å3, $R1 = 2.864$ and, (B) ZIF–BSA: *cubic*, $a = 16.350$ (1) Å; $V = 4370.72$ (6) Å3, $R1 = 2.859$ (Fig. 2).

The X-ray diffraction (XRD) patterns for ZIF-8 are in an agreement with those reported from the literature (Watson et al. 2002; Pan et al. 2011; Gross et al. 2012; Kida et al. 2013). The main indices of all X-ray diffraction peaks (011, 002, 112, 013, and 222) to a sodalities structure have shown excellent concordance with crystal formation, as reported previously (Watson et al. 2002; Pan et al. 2011; Gross et al. 2012; Kida et al. 2013) (Fig. 2: ZIF–BSA a). However, there was only a small decrease in intensity of the peak for the ZIF–BSA as BSA was adsorbed on the surface of ZIF-8 crystals. ZIF–BSA X-ray diffraction spectra showed peaks at 37.2° and 43.6° (Fig. 2: ZIF–BSA **b**). Moreover, the X-ray diffraction analysis also showed that hybrid materials exhibited all X-ray diffraction peaks of ZIF-8, but at lower intensities. In addition, SEM analysis

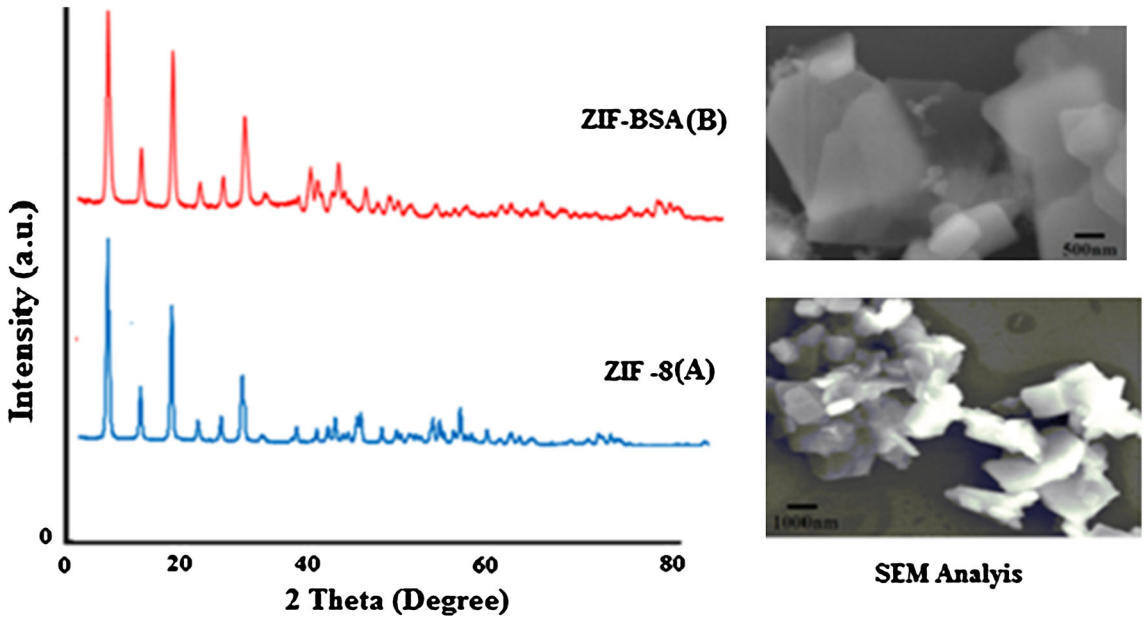

Fig. 2 X-ray diffraction spectrum analysis: **a** synthesized zeolites imidazole framework (ZIF-8), and **b** zeolites imidazole framework–bovine serum albumin (ZIF–BSA) composite in aqueous medium

of the ZIF-8 crystal (10–100 nm) and ZIF–BSA crystal (15–100 nm) confirmed the encapsulation to be the same as shown in Fig. 2. It thus appears that the growth kinetics of ZIF-8 may be repeated with ZIF–BSA because of fast homogeneous nucleation in both cases (pure and hybrid materials). In addition, hybrid crystals have a similar shape compared to those of ZIF-8, which reflects the overall result of the faster homogeneous nucleation growth. Likewise, recent studies clearly indicated that ZIF-8 was able to easily adsorb molecules that have a much larger size than their window (3.4 Å) size (Watson et al. 2002; Pan et al. 2011; Gross et al. 2012; Kida et al. 2013).

Optical and electron microscope analysis

The results of optical and electron microscope analysis suggest that the BSA/FITC was enriched at the inner interface of ZIF-8 through successive adsorption. This enrichment may be associated with fast homogenous nucleation during synthesis of ZIF-8 and the polar nature of BSA. TEM images clearly indicated the presence of a composite material that contained unmodified BSA within the ZIF-8 crystal surface. This may be due to the sodalite topology consisting of cavities of 11.6 Å diameter connected by eight 3.4 Å windows. Initially, studies have shown that ZIF-8 can easily adsorb molecules much larger than its window size. It directly confirmed the occurrence of encapsulation Watson et al. 2002; Pan et al. 2011; Gross et al. 2012; Kida et al. 2013). TEM images of blank ZIF-8 crystal (of less than 15 nm) are also shown in Fig. 3a. The presence of BSA (2–4 nm) in ZIF-8 was also confirmed by TEM analysis with electron diffraction pattern (Fig. 3b). TEM monographs of ZIF-8 polyhedral crystals were also compared with the previous results tested through other microscopy and spectroscopy techniques (Watson et al. 2002; Pan et al. 2011; Gross et al. 2012; Kida et al. 2013).

Imaging by a confocal laser scanning microscope (CLSM) supported the presence of aggregated FITC–BSA in ZIF-8 hybrid crystal, as shown in Fig. 4. The extremely bright spots, which came from the fluorescence of FITC–BSA, were highly visible at every location of the aggregates (Fig. 4a–d). The analysis of the aggregate sizes is very convoluted in the sample examined through the optical microscope. Moreover, the concentration of incorporated BSA was not expected to exceed the bulk concentration. The aggregate CLSM images show a bright fluorescence at the location of the BSA–FITC, indicating that there was strong enrichment of BSA–FITC in the hybrid crystal.

Spectroscopy analysis

The pure synthesized form of ZIF-8 (III), pure BSA (II), and composite of ZIF–BSA (I) were analyzed using UV–visible and infrared spectroscopy, as shown in Figs. 5 and 6. The UV–Vis and IR spectra of pure ZIF-8 in aqueous media are comparable to those reported previously (Watson et al. 2002; Wittemann et al. 2007; Pan et al. 2011; Gross et al. 2012; Kida et al. 2013). The UV–Vis spectrum of purchased ZIF-8 was recorded to have an absorption peak at 209 nm (Fig. 5a) while the absorption peak of BSA appeared at 279 nm, as shown in Fig. 5b. This value matched with those cited previously (Watson et al. 2002; Wittemann et al. 2007; Tan et al. 2010; Bux et al. 2011; Pan et al. 2011; Gross et al. 2012; Kida et al. 2013). Upon encapsulation of BSA and FITC–BSA in ZIF-8, the

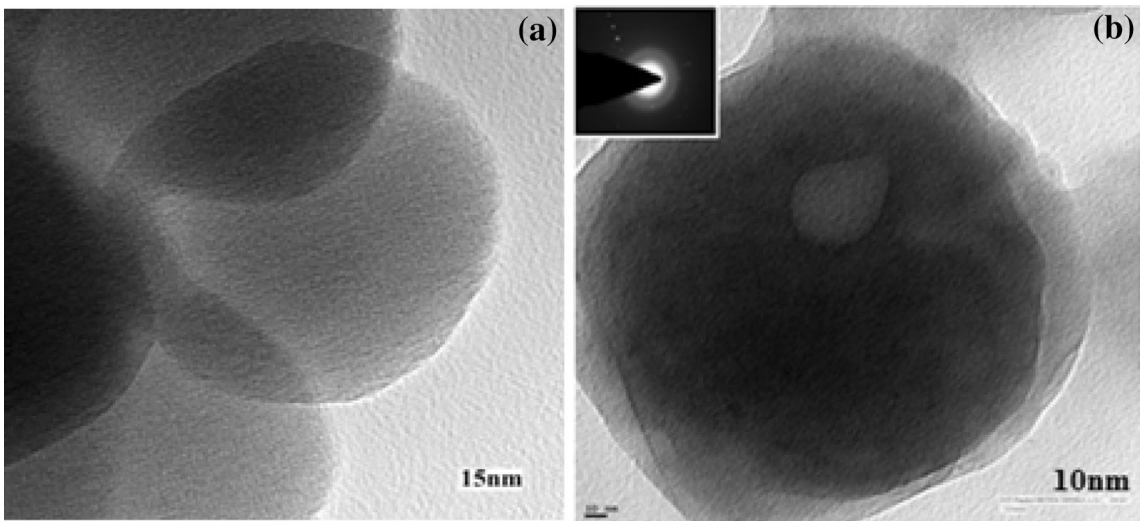

Fig. 3 HRTEM images of encapsulation of protein in zeolitic imidazolate framework, **a–c** high magnification image of blank crystals and homogeneous distribution of protein-containing hybrid crystal prepared in aqueous solution: **a** blank crystal and **b** hybrid crystals containing BSA (2–3 nm) with electron diffraction pattern

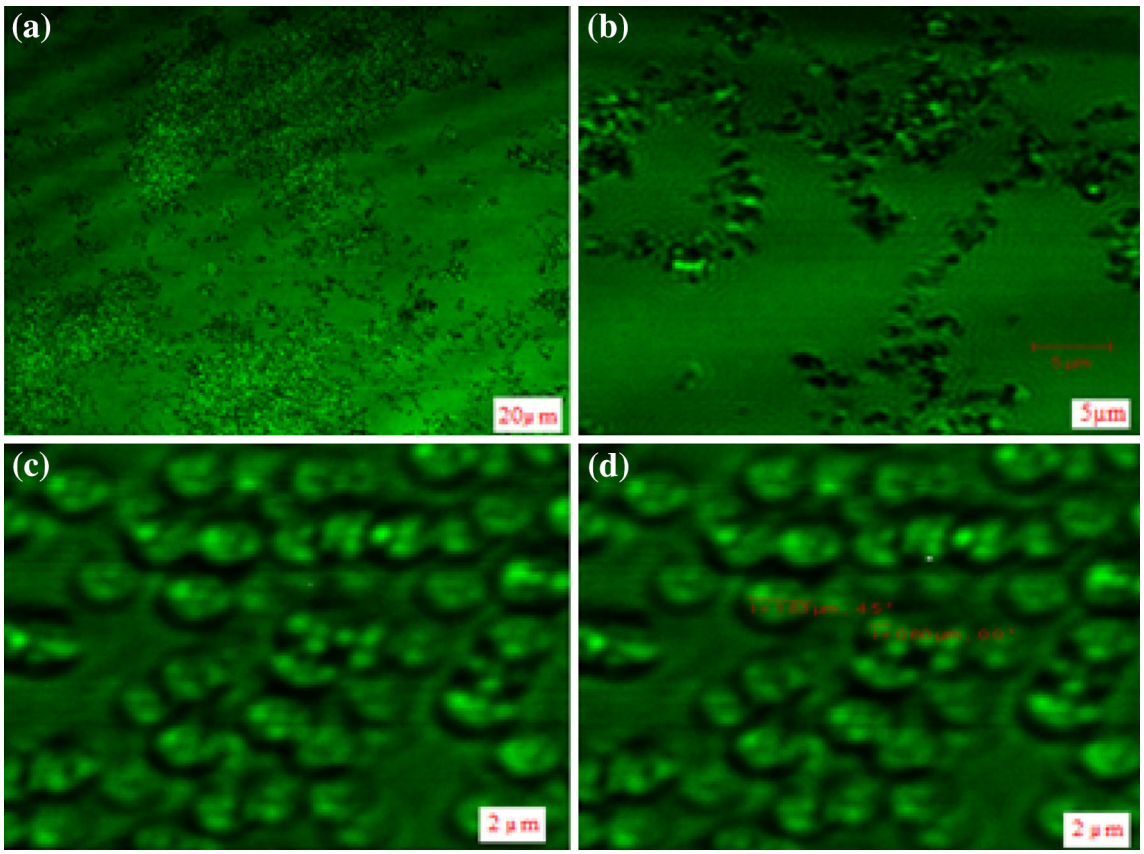

Fig. 4 CLSM images of ZIF–BSA–FITC aggregates with immobilized FITC–BSA. The organic dye (*green color*) was used as a fluorescent probe for globular protein in the ZIF-8 hybrid crystal. The micrographs and their individual *green* channels referring to the fluorescence of FITC–BSA were taken at three different magnifications (2, 5, and 20 μm), as indicated by the *bars*

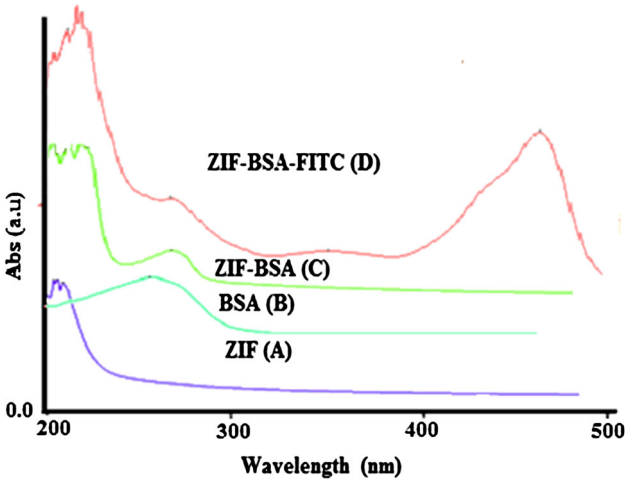

Fig. 5 UV-Vis absorption spectra of **a** pure ZIF-8 in distilled water, **b** pure BSA in distilled water, **c** composite of ZIF–BSA in aqueous medium, and **d** composite of ZIF–BSA–FITC in aqueous medium

presence of notable absorption peaks was apparent at the low wavelengths of 209 and 279 nm (Fig. 5c, d). Such an occurrence suggests that encapsulation happened within ZIF-8. A detailed explanation of this phenomenon has already been sought (Watson et al. 2002; Wittemann et al. 2007; Tan et al. 2010; Bux et al. 2011; Pan et al. 2011; Gross et al. 2012; Kida et al. 2013); however, the encapsulation may not have been completed, as separate absorption peaks can also be observed for ZIF-8 and BSA in the reported spectra. It may be due to the proper functionalization or conjugation of the ZIF-8 with BSA (Watson et al. 2002; Wittemann et al. 2007; Tan et al. 2010; Bux et al. 2011; Pan et al. 2011; Gross et al. 2012; Kida et al. 2013).

According to the FTIR analysis, IR peaks were found between 900 and 1400 cm^{-1} with the absorption of C–N bonds (Fig. 6). In addition, the absorption band at 2928 cm^{-1} was associated with aromatic C–H stretching, while that of 3134 cm^{-1} was associated with the aliphatic C–H stretch of the imidazole in pure ZIF-8 crystal. Basically, Zn–N stretching is shown by absorption bands at 421 cm^{-1} in the IR spectrum. The peaks of pure BSA also matched well, as recognized previously (Watson et al. 2002; Wittemann et al. 2007; Tan et al. 2010; Bux et al. 2011; Pan et al. 2011; Gross et al. 2012; Kida et al. 2013). The absorption spectrum of BSA exhibited three apparent absorption bands at 1654, 421, and 3284 cm^{-1}, which are

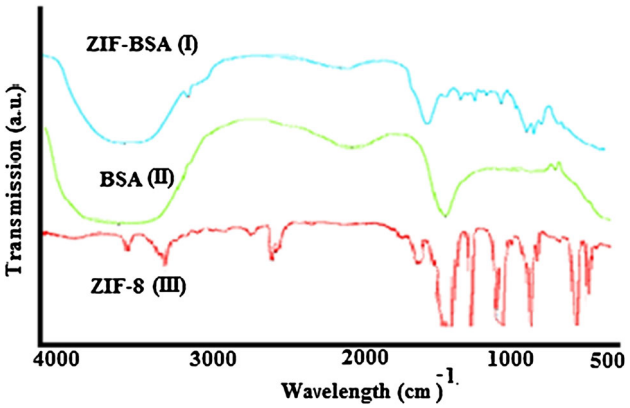

Fig. 6 FTIR analysis of pure synthesized ZIF-8, pure BSA and BSA/ZIF-8 mixed conjugates with loadings marked above the *curves*

assigned to three amide types of I (Zn–N stretching mode), II (N–H bending mode), and III (C–N stretching mode and N–H bending mode), respectively. The presence of BSA/ZIF-8 composite thus indicated that there were strong chemical interactions between the ZIF-8 and BSA. The fundamental OH stretching vibration (3600–3000 cm^{-1}) was also evident in the IR spectrum. The strong peaks at the 1654 cm^{-1} band confirmed the formation of BSA–ZIF-8 composite. The lack of absorption peak for pure ZIF-8 also confirmed the presence of BSA within ZIF-8 crystals.

Discussion

Protein encapsulation methods can help, when conducted with nano materials, to counter significant challenges including (1) effective control over composition along with shape and size of porous materials, (2) spatial distribution of nanomaterials inside the pore and framework, and (3) perseverance of the chemical and physical properties of these porous materials for possible industrial applications (Watson et al. 2002; Wittemann et al. 2007; Tan et al. 2010; Bux et al. 2011; Pan et al. 2011; Gross et al. 2012; Kida et al. 2013). Likewise, in this study, BSA encapsulation processes in ZIF-8 helped us explore the fundamental issues to resolve various challenges in biomedical applications.

In this report, the encapsulation mechanism consisted of fast homogeneous nucleation crystal growth of ZIF-8, and these forming crystals supported the successive adsorption of BSA during the synthesis process only. Moreover, we found that this encapsulation strategy succeeded only when BSA was introduced after the reaction proceeded, but not when it was introduced immediately upon the initiation of the reaction (Wittemann et al. 2007; Tan et al. 2010; Bux et al. 2011; Pan et al. 2011). Therefore, we assumed that the crystallization process was favored by the fast homogeneous nucleation of ZIF-8 in the presence of bovine serum albumin (BSA) in aqueous medium. In other words, BSA-induced heterogeneous nucleation was not dominant over the entire incorporation process.

In addition, cross investigation performed using FITC-labeled BSA/ZIF-8 crystal under the same experimental conditions suggested that the incorporation process was based only on successive adsorption of free BSA by the continuous formation of hollow crystals or co-ordination polymer spheres toward the end of the reaction [24–28]. Consequently, it can be inferred that the polar nature of BSA not only supported the adsorption on the solid surface, but also enhanced the affinity of spheres through weak coordination interactions with the framework of ZIF-8. Accordingly, the synthesis of hybrid composites confirmed the stable encapsulation of protein or BSA within ZIF-8 crystals. These findings suggest that the synthesized hybrid composite material would maintain desirable active properties in the ZIF-8 crystals including catalytic, conductive (due to BSA), molecular sieving, and regioselective guest reactivity, as well as having thermal stability. Finally, such biostorage by porous materials (i.e., ZIF-8) could possibly offer robustness to the biomolecules stored within for diverse biotechnological and/or pharmaceutical applications.

Conclusion

An experimental study was carried out to demonstrate a suitable and effective procedure for encapsulating proteins within an assembled porous crystal material. As this approach is expected to be feasible for a wide range of proteins or other biomolecules, it may be possible to expand its potential applications to various relevant fields. The success of our case study for encapsulation of protein (BSA) in a ZIF-8 matrix thus allows researchers to take full advantage of ZIF-8 with its unique properties of thermal stability, porous structure, and molecular sieving behavior. More studies in this field are needed to validate and expand the practical applicability of ZIF-8 or other MOFs.

Acknowledgments We are grateful to the Director of CSIR-CSIO, Chandigarh, India for supporting this research. The fifth author acknowledges an India grant (OMEGA/PSC0202) from CSIR, India. The first, second and sixth authors also acknowledge the financial grant from the National Research Foundation of Korea (NRF) funded by the Ministry of Education, Science, and Technology (MEST) (No. 2009-0093848).

References

Allendorf MD, Bauer CA, Bhakta RK, Houk RJT (2009) Luminescent metal–organic frameworks. Chem Soc Rev 38(5):1330–1352

Buso D, Nairn KM, Gimona M, Hill AJ, Falcaro P (2011) Fast synthesis of MOF-5 microcrystals using Sol–Gel SiO_2 nanoparticles. Chem Mater 23(4):929–934

Bux H, Feldhoff A, Cravillon J, Wiebcke M, Li YS, Caro J (2011) Oriented zeolitic imidazolate framework-8 membrane with sharp H2/C3H8 molecular sieve separation. Chem Mater 23(8):2262–2269

Chen B, Xiang S, Qian G (2010) Metal–organic frameworks with functional pores for recognition of small molecules. Acc Chem Res 43(8):1115–1124

Czaja AU, Trukhan N, Müller U (2009) Industrial applications of metal–organic frameworks. Chem Soc Rev 38(5):1284–1293

Danhier F, Ansorena E, Silva JM, Coco R, Le Breton A, Préat V (2012) PLGA-based nanoparticles: an overview of biomedical applications. J Control Release 161(2):505–522

Gao J, Gu H, Xu B (2009) Multifunctional magnetic nanoparticles: design, synthesis, and biomedical applications. Acc Chem Res 42(8):1097–1107

Gross AF, Sherman E, Vajo JJ (2012) Aqueous room temperature synthesis of cobalt and zinc sodalite zeolitic imidizolate frameworks. Dalton Trans 41(18):5458–5460

Kida K, Okita M, Fujita K, Tanaka S, Miyake Y (2013) Formation of high crystalline ZIF-8 in an aqueous solution. CrystEngComm 15(9):1794–1801

Lee J, Mahendra S, Alvarez PJ (2010) Nanomaterials in the construction industry: a review of their applications and environmental health and safety considerations. ACS Nano 4(7):3580–3590

Liu B (2012) Metal–organic framework-based devices: separation and sensors. J Mater Chem 22(20):10094–10101

Lohe MR, Gedrich K, Freudenberg T, Kockrick E, Dellmann T, Kaskel S (2011) Heating and separation using nanomagnet-functionalized metal–organic frameworks. Chem Commun 47(11):3075–3077

Lu G, Li S, Guo Z, Farha OK, Hauser BG, Qi X, Huo F (2012) Imparting functionality to a metal–organic framework material by controlled nanoparticle encapsulation. Nat Chem 4(4):310–316

McKinlay AC, Morris RE, Horcajada P, Férey G, Gref R, Couvreur P, Serre C (2010) BioMOFs: metal–organic frameworks for biological and medical applications. Angew Chem Int Ed 49(36):6260–6266

Pan Y, Liu Y, Zeng G, Zhao L, Lai Z (2011) Rapid synthesis of zeolitic imidazolate framework-8 (ZIF-8) nanocrystals in an aqueous system. Chem Commun 47(7):2071–2073

Park KS, Ni Z, Côté AP, Choi JY, Huang R, Uribe-Romo FJ, Yaghi OM (2006) Exceptional chemical and thermal stability of zeolitic imidazolate frameworks. Proc Natl Acad Sci 103(27):10186–10191

Phan A, Doonan CJ, Uribe-Romo FJ, Knobler CB, O'keeffe M, Yaghi OM (2010) Synthesis, structure, and carbon dioxide capture properties of zeolitic imidazolate frameworks. Acc Chem Res 43(1):58–67

Pinto Reis C, Neufeld RJ, Ribeiro AJ, Veiga F (2006) Nanoencapsulation II. Biomedical applications and current status of peptide and protein nanoparticulate delivery systems. Nanomedicine 2(2):53–65

Springuel-Huet MA, Nossov A, Guenneau F, Gédéon A (2013) Flexibility of ZIF-8 materials studied using 129 Xe NMR. Chem Commun 49(67):7403–7405

Such GK, Johnston AP, Caruso F (2011) Engineered hydrogen-bonded polymer multilayers: from assembly to biomedical applications. Chem Soc Rev 40(1):19–29

Sugikawa K, Furukawa Y, Sada K (2011) SERS-active metal–organic frameworks embedding gold nanorods. Chem Mater 23(13):3132–3134

Tan JC, Bennett TD, Cheetham AK (2010) Chemical structure, network topology, and porosity effects on the mechanical properties of Zeolitic Imidazolate Frameworks. Proc Natl Acad Sci 107(22):9938–9943

Tsuruoka T, Kawasaki H, Nawafune H, Akamatsu K (2011) Controlled self-assembly of metal–organic frameworks on metal nanoparticles for efficient synthesis of hybrid nanostructures. ACS Appl Mater Interfaces 3(10):3788–3791

Watson MS, Whitaker MJ, Howdle SM, Shakesheff KM (2002) Incorporation of proteins into polymer materials by a novel supercritical fluid processing method. Adv Mater 14(24):1802–1804

Wittemann A, Azzam T, Eisenberg A (2007) Biocompatible polymer vesicles from biamphiphilic triblock copolymers and their interaction with bovine serum albumin. Langmuir 23(4):2224–2230

Worsdoorfer B, Pianowski Z, Hilvert D (2012) Efficient in vitro encapsulation of protein cargo by an engineered protein container. J Am Chem Soc 134:909–911

Yeo Y, Park K (2004) Control of encapsulation efficiency and initial burst in polymeric microparticle systems. Arch Pharmacal Res 27(1):1–12